An Incorporated Control Strategy of Commutation and Conduction Torque Ripples Mitigation for BLDCM Drives in Household Appliances

JIADAN WEI [ID], (Member, IEEE), PENG LIU, AND WENJIE TAO

Electrical Engineering Department, College of Automation Engineering, Nanjing University of Aeronautics and Astronautics, Nanjing 211106, China

Corresponding author: Jiadan Wei (weijiadan@nuaa.edu.cn)

ABSTRACT In this paper, an incorporated control strategy of both commutation and conduction torque ripples mitigation for brushless DC machine (BLDCM) with the sinusoidal back electromotive force(EMF) is proposed to reduce the vibration and noise of household appliances for higher comfortable capability. Based on the combined torque ripple analysis with respect to the stator flux linkage trajectory, a three-phase voltage vector injection (TVVI) method is designed and implemented in the commutation interval to compensate the sharp dips of the stator flux trajectory for the mitigation of the commutation torque ripple, and duty cycle of the injected voltage vector could be regulated automatically. Then, a simple direct power control (DPC) method with TVVI in the PWM modulation is employed as inner-loop for BLDCM to obtain the desired waveforms of currents with the specific dc-link current sampling method, and the reduction of both conduction and commutation torque ripples is achieved. The proposed incorporated control strategy is validated through simulation experiment results, and the effect on the torque ripples are compared with the traditional approaches.

INDEX TERMS Incorporated control strategy, commutation and conduction torque ripples mitigation, direct power control, three-phase voltage vector injection, stator flux trajectory.

I. INTRODUCTION

BLDCM has been utilized widely for household electrical appliances due to the merits of high power density, simple structure, easy control, and low cost. However, the inherent torque ripples due to the quasi-square wave current control result in the vibration and noise, and it is not suitable to be utilized in the restrict applications where the noise and smooth instantaneous torque are of major concerns for the comfortable performance. The main reasons of torque ripples in BLDCM have been summarized as follows:

(1) The different current slewing rates of incoming and outgoing phase in the commutation interval, then the deviated current resulted in the non-commutating phase is inevitable, and the induced torque ripple is defined as commutation torque ripple.

(2) The imperfect machine design and manufacture lead to the non-ideal trapezoidal back EMF even the sinusoidal waveforms, the traditional quasi-square wave currents by the chopping control scheme generate the torque ripple in the normal conduction interval, and this kind of torque ripple is defined as the conduction torque ripple.

Furthermore, some of the PWM patterns for the voltage source inverter(VSI) bring the undesired freewheel currents in the un-conducting phase windings, and the generated torque ripple which is equal to the product of the freewheel current and corresponding back EMF deteriorates the output torque in the conduction interval, and this torque ripple could also be sorted into conduction torque ripple.

In general case, commutation torque ripple of BLDCM usually causes a relatively worse effect, even leads to a significant torque ripple up to 50% of the average torque, thereby the mitigation for the commutation torque ripple is of great interest in the recent literature. R. Carlson deduced

---

The associate editor coordinating the review of this manuscript and approving it for publication was Amin Hajizadeh.

that the different current slew rates between the incoming phase and the outgoing phase are the main reason for commutation torque ripple [1], then, various PWM techniques are exploited to reduce the current slew rate of the faster one between the incoming and outgoing phase to keep the non-commutating phase current constant during the commutation period [2]–[4], these approaches work effectively in the low and intermediate speed range with the overlap angle control method [5], whereas at the high speed, especially under the rated power condition, the PWM methods could not effectively reduce the commutation torque ripple due to finite dc-link voltage of VSI. A 180° switching mode at higher speeds for the reduction of both torque ripple magnitude and commutation time is proposed in [6] and an optimized combination of PWM modulation patterns in the different ranges is given in [7] for the smooth torque control in full speed range. Literatures [8]–[11] adopt an extra DC-DC converters to compensate the dc-link voltage during the commutation interval for the torque ripples mitigation, however, the cost, volume and the control complexity of the system are greatly increased for the commutation torque ripple mitigation, moreover, and the conduction torque ripple due to the non-ideal back EMF has not been considered in these methods.

Thus, the coordinate transformation and direct torque control(DTC) algorithms for the AC motors were extended to mitigate the conduction torque ripples of BLDCM with the non-ideal trapezoidal back EMF in the literature [12]–[15]. An on-line back-EMF estimation technique is used to inject appropriate phase currents to compensate non-ideality of the back-EMF waveform in [16]. Furthermore, the current optimization control methods applying integral variable structure and model predictive control are also proposed in [17]. However, the estimation of accurate rotor position and instantaneous torque by various observers increase the control complexity and it is difficult and expensive to be carried out, furthermore, the estimation error of rotor position and motor parameters which are varying with respect to the operating conditions may result in undesired torque ripples.

Direct power control(DPC), which is the most popular high-performance control method for PWM rectifiers with the advantages of simple structure and rapid dynamic response [18], [19], has been considered for the torque ripple reduction of BLDCM in literature [20], [21], where the direct power control loop based on the two-vector finite control-set model-based predictive control approach is employed to replace the traditional inner loop and PWM generation module. Although the better steady-state performance of the output torque over a wide speed range could be achieved, the high bandwidth controller is required to cope the torque ripple frequencies, while, the commutation torque ripple could not be reduced obviously, and the control complexity of proposed BLDCM driving system is also increasing.

As aforementioned, in order to achieve the improvement of the output torque performance of BLDCM, the commutation and conduction torque ripples could be mitigated by the different complex control methods for the corresponding

torque ripples, where, the merits of simple structure and control method for BLDCM are weakened. Moreover, the recent literature is focused on the certain torque ripples of BLDCM, while, there are two different kinds of torque ripples of BLDCM with the non-ideal trapezoidal back EMF. Therefore, in this paper, unlike the above-separated mitigation methods of commutation and conduction torque ripples for BLDCM with non-ideal trapezoidal back EMF, a novel incorporated torque ripples mitigation strategy is proposed. A simple direct power control(DPC) scheme instead of the traditional current control is employed as the inner-loop control, where the constant output power could ensure the constant output torque by the corresponding waveforms implementation of phase currents in the steady state, then, the conduction torque ripples of BLDCM due to non-ideal trapezoidal back EMF could be eliminated. In order to achieve the elimination of commutation torque ripple, a three-phase voltage vector injection(TVVI) method which refers to the five-step SVPWM is employed in PWM modulation module of the inner-loop DPC control, where the active three-phase voltage vector is intentionally arranged for the compensation of the sharp dips of stator flux linkage trajectory. Although the property of TVVI method is similar to the traditional overlap angle control for BLDCM, the duty cycle calculation of the injected voltage vector has been derived, then, the incorporated method for the mitigation of both conduction and commutation torque ripples could be obtained, moreover, a simplified implementation method for the proposed BLDCM is also achieved herein.

Thus, the manuscript is organized as follow. The relations between the active voltage vectors and flux linkage trajectory is given in section II for torque ripple analysis of BLDCM with non-ideal trapezoidal back EMF, then, in section III, the three-phase voltage vector injection (TVVI) method for the commutation torque ripple is proposed for BLDCM with the PWM-ON pattern, and this TVVI method is also extended to the BLDCM with other PWM patterns. In section IV, the proposed incorporated torque ripple mitigation method with the TVVI and simple direct power control(DPC) is designed for the high output torque performance of BLDCM. Simulation and experiment results are presented to illustrate the validity and effectiveness of the proposed incorporated control strategy in section V and VI. Finally, the conclusion is drawn in section VII.

II. STATOR FLUX LINKAGE TRAJECTORY FOR TORQUE RIPPLE ANALYSIS

In order to mitigate the torque ripples of BLDCM with the sinusoidal back EMF, the stator flux linkage trajectory should be circle-shaped as far as possible due to the general torque expression

$$T_e = K_t \psi_s \psi_r \sin \delta \qquad (1)$$

where, ψ_s and ψ_r represent the stator and rotor flux linkage respectively, δ indicates the phase angle between the stator and rotor flux linkage, and K_t is the torque coefficient. At the

constant speed region of BLDCM with the determined load, the rotor flux linkage ψ_r and δ could be assumed as a constant value, then the torque is proportional to the stator flux linkage ψ_s. Unlike the conventional literature of [19]–[21] with respect to current slewing rate analysis for the torque ripples of BLDCM, the stator flux linkage trajectory is employed to discuss the torque ripples herein.

The stator flux linkage of the phase windings is shown as

$$\psi_s = \int (V_s - i_s R_s)dt \qquad (2)$$

where, V_s refers to the synthesized voltage of the three-phase windings, i_s and R_s are defined as the phase current and resistance respectively. Usually, R_s could be negligible, since the BLDCM works in the rated speed in the household appliances, and the stator flux linkage can be simplified to be the integration of the synthesized voltage.

In the conventional two-phase conduction mode of BLDCM, there are a total six active voltage vectors which could be represented as U_{A+B-}, U_{A+C-}, U_{B+C-}, U_{B+A-}, U_{C+A-} and U_{C+B-}, as shown the red solid line in Fig.1(a), and the symbols '+' and '−' in the subscript stand for that the corresponding phase windings connect to the positive and negative point of DC-link power source, respectively, thus, subscript A+B− corresponds to the conduction mode that the phase winding A is connected to the positive point of DC-link, and the phase winding B is connected to the negative point of the DC-link, and so on the other subscripts of the active voltage vectors. The synthesized voltage for the stator flux linkage is determined by the corresponding active voltage vectors and the back EMF of the un-conducting phase winding in each 60 electrical degrees conduction mode, which is defined as segment ①, ②, . . . , ⑤, ⑥ shown in Fig.1(a).
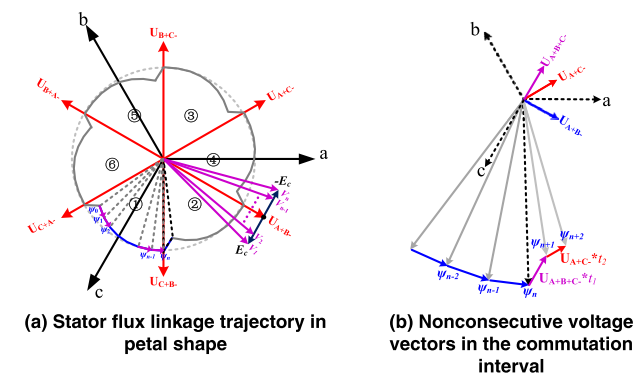

(a) Stator flux linkage trajectory in petal shape

(b) Nonconsecutive voltage vectors in the commutation interval

FIGURE 1. Schematic diagram of the stator flux linkage trajectory of BLDCM with the two-phase conduction scheme.

In segment ①, the stator flux linkage is determined by the synthesized voltage vector of U_{A+B-} and the back EMF of phase C, where the voltage vector U_{A+B-} is constant, while the back EMF of outgoing phase C varies in the conduction interval. Thus, the synthesized voltages can be represented as $V_{1,2,...,n-1,n}$, as shown in Fig.1(a) in purple solid lines, ψ_0 is the initial value of the stator flux linkage in the segment ①,

the stator flux linkage can be presented as follow

$$\begin{aligned} \psi_k &= \psi_{k-1} + \int V_k \cdot dt \\ &= \psi_{k-1} + V_k \cdot \Delta t \quad (k = 1, 2..., n-1, n) \end{aligned} \qquad (3)$$

where, Δt is the sampling period for the synthesized voltages. Due to the variation of the back EMF of the un-conducting phase C, flux linkage varies from the original ψ_0 to the ψ_n consecutively in the conduction mode, then, the stator flux linkage trajectory in segment ① is illustrated in Fig.1(a) with the blue solid line, the amplitude of the stator flux linkage increases non-linearly along with the integration of the synthesized voltages, which is vertical to the flux linkage.

While, in the commutation interval, the active voltage vector suddenly switches from U_{A+B-} to U_{A+C-}, and a new voltage vector U_{A+B+C-} takes effect due to the freewheeling current of the outgoing phase B, therefore, the commutation interval could be divided into two parts t_1 and t_2, where the active voltage vector is U_{A+B+C-} and U_{A+C-} respectively, and it results in a sharp dip of stator flux linkage locus due to the nonconsecutive voltage vectors, as shown in Fig.1(b). Since the rotor speed is assumed to be constant in the steady-state, the torque ripples occur in each segment of BLDCM with the sinusoidal back EMF according to the equation(1). Moreover, there is only one voltage vector can be utilized in each segment of BLDCM with the two-phase conduction scheme, the amplitude of stator flux linkage could not be easily controlled due to the variability of the back EMF of the un-conducting phase windings. Furthermore, sharp dips in the stator flux linkage at every commutation interval are depended on many factors, such as motor speed, dc-link voltage, motor parameters, PWM patterns for inverter and the amount of the load.

Thus, the key issue in the torque ripples mitigation of BLDCM with the sinusoidal back EMF in the constant speed region is to control the tendency of the stator flux linkage to match with the circle-shaped rotor flux linkage for the smooth output torque. Although the trajectory of stator flux linkage could be adjusted in the circle shape for the ac motors such as permanent magnet synchronous machine and induction machine by the vector control or DTC schemes [22], [23], the accurate rotor position should be detected or estimated for the selection of the consecutive voltage vectors, whereas it is considered to be cumbersome for the BLDCM. Thus, the specific voltage injection method should be adopted for the curve compensation of the stator flux linkage [24].

III. THREE-PHASE VOLTAGE VECTOR INJECTION(TVVI) FOR COMMUTATION TORQUE RIPPLE

In the conventional commutation torque ripple analysis of BLDCM, the essence of commutation torque ripple is the inequality between the decreasing current rate of the outgoing phase and the increasing current rate of the incoming phase, therefore, the non-commutating phase current varies during the commutation intervals. Taking the commutation interval from A+B− to A+C− in the PWM-ON pattern for
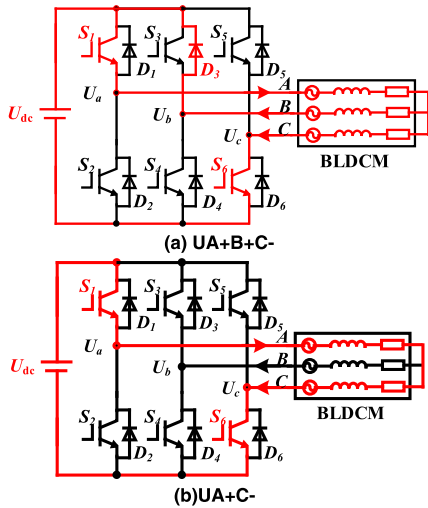
FIGURE 2. The active voltage vectors in the commutation interval from A+B− to A+C−.

an example, A+B− stands for positive current of phase A and negative current of phase B, and A+C− refers to the positive current of phase A and negative current of phase C. Phase B is the outgoing phase and phase C is the incoming phase, phase A is the non-commutating phase in the commutation interval from A+B− to A+C−. The current flowing path in the commutation interval is shown in Fig.2(a), S_1 keeps on for phase A in the PWM-ON pattern, and current of phase B free-wheels through D_3, S_6 works in PWM mode. When S_6 is on, the active voltage vector is $U_{A+B+C−}$, while S_6 is off, the voltage vector is zero vector U_{A+B+C+}, which has no effect on the flux linkage. Another active voltage vector is U_{A+C} after the free-wheeling of phase B shown in Fig.2(b). Therefore, the corresponding stator flux linkage with respect to the active voltage vectors of $U_{A+B+C−}$ and U_{A+C} is shown in Fig.1(b), and the sharp dip of flux is obvious, it will lead to the commutation torque ripples.

In the literature for the mitigation of the commutation torque ripples [3], the slewing rate of each phase current neglecting the resister could be derived as

$$\begin{cases} \dfrac{di_a}{dt} = \dfrac{d_6 U_{dc}}{3l_a} + \dfrac{e_b + e_c - 2e_a}{3l_a} \\ \dfrac{di_b}{dt} = \dfrac{d_6 U_{dc}}{3l_b} + \dfrac{e_a + e_c - 2e_b}{3l_b} \\ \dfrac{di_c}{dt} = \dfrac{-2d_6 U_{dc}}{3l_c} + \dfrac{e_a + e_b - 2e_c}{3l_c} \end{cases} \quad (4)$$

where, $U_x, i_x, e_x, l_x(x = a, b, c)$ indicate the phase voltages, phase currents, back EMFs and inductances of three-phase windings respectively, d_6 is duty cycle of S_6.

The current changing rate of the outgoing phase B and incoming phase C should be identical, in other words, the current of non-commutating phase A could be regulated as constant in the commutation interval. At the low-speed range, where $U_{dc} > 2 e_a − e_b − e_c$, the slewing rate of phase A is greater than 0 when $d_6 = 1$, whereas $d_6 = 0$, it is less than 0,

thus the current of phase A could be regulated as constant by the duty cycle d_6. However, in the high-speed range, where $U_{dc} < 2 e_a − e_b − e_c$, di_a/dt is always negative, and there will be a current drop of the non-commutating phase in the commutation interval, and it could not be regulated by the duty cycle d_6. From the current waves shown in Fig.3, it can be seen that the decreasing current rate of the outgoing phase B is higher than the increasing current rate of the incoming phase C, the non-commutating current decreases during the commutation interval, then the commutation torque ripples occur.
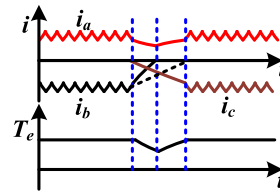

FIGURE 3. Schematic diagram of the three-phase currents in the commutation interval at high speed.

The aforementioned theoretical derivation of commutation torque ripples mitigation is based on the assumption of ideal trapezoidal back EMF, and it is not suitable for the BLDCM with the sinusoidal back EMF. From the stator flux linkage waveform in Fig.1(b), due to the square waveform current control method, the available active voltage vectors are limited, and the sharp dip of flux is inevitable. Therefore, further approaches should be employed for the circle flux linkage regulation to achieve the commutation torque ripple mitigation.

A. THREE-PHASE VOLTAGE VECTOR INJECTION METHOD

During the commutation interval from A+B− to A+C−, a three-phase voltage vector, which is defined as A+B−C−, is exploited for the changing of current slewing rate. Switch S_4 turns on for the outgoing phase B, the free-wheeling current is actively controlled and the current flowing path is shown in Fig.4. The amplitudes of the corresponding phase voltages are $U_a = U_{dc}$, $U_b = 0$, and $U_c = 0$ respectively, then, the current slewing rate of the non-commutating phase A could be derived as

$$\frac{di_a}{dt} = \frac{2U_{dc}}{3l_a} - \frac{2e_a - e_c - e_b}{3l_a} > \frac{2U_{dc}}{3l_a} - \frac{4E_m}{3l_a} > 0 \quad (5)$$

where, E_m is defined as the maximum value of back EMF, and $2e_a − e_c − e_b < 4 E_m$, U_{dc} should be large than $2^* E_m$, then, the above equation (5) denotes that the current slewing rate of non-commutating phase A is larger than 0 in the commutation interval from A+B− to A+C−. It is of worth for the regulation of phase current A, especially in the high-speed range, and the non-commutating phase current could remain constant.

Since the injected voltage vector of the TVVI method, the stator flux linkage trajectory of BLDCM in the commutation interval has been modified to be shown in Fig. 5,
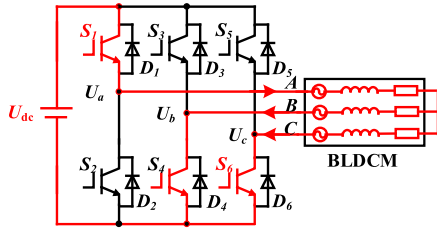
FIGURE 4. The current flowing path in the commutation interval when voltage vector A+B−C− is injected.
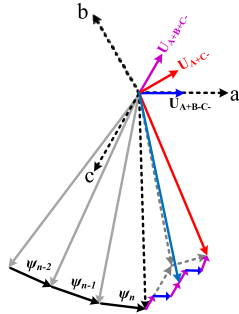

FIGURE 5. The improved flux linkage trajectory of BLDMC in the commutation interval from A+B− to A+C−.

the corresponding flux linkage of BLDCM in each duty cycle has been enlarged for the compensation of the dips of the flux linkage trajectory due to the injected voltage vector A+B−C− in blue color, which tends to be the circle curve for the smooth output torque according to the equation(1). Although it seems to get the circle curve of flux linkage as the direct torque control strategy, the proposed TVVI method is easier to be implemented for BLDCM.
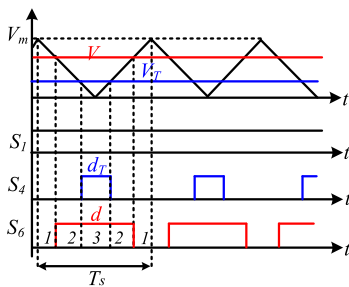

FIGURE 6. Schematic diagram of three-phase voltage vector injection in the commutation interval.

Fig.6 illustrates the implementation of the three-phase voltage vector injection (TVVI) method in the commutation interval from A+B− to A+C−. In the normal operation mode, S_1 keeps on in the commutation interval. V is the output of the regulator for the inner loop of DPC, and it is compared with the carrier wave for the duty cycle d to control the switch S_6. There are only two different operation modes in the commutation interval when S_1 and S_6 turn on, the active voltage vector is defined as 2, and the current slewing rate of

phase A can be deduced as

$$\frac{di_{a2}}{dt} = \frac{U_{dc}}{3l_a} + \frac{e_b + e_c - 2e_a}{3l_a} \quad (6)$$

While S_1 turns on and S_6 turns off, the active voltage vector is defined as 1, and the current slewing rate of phase A can be derived as

$$\frac{di_{a1}}{dt} = \frac{e_b + e_c - 2e_a}{3l_a} \quad (7)$$

The three-phase voltage vector injection method could be implemented by the chopping control of the switch S_4, and the duty cycle d_T for S_4 is determined by the extra modulation wave V_T, which should be lower than V. Thus, the PWM operation mode of the inverter is analogous to the five-step SVPWM method, and the proposed three-voltage vector 3 is injected in the middle of the PWM period, the other two-phase voltage vectors are distributed symmetrically to the dual sides of intermediate voltage vector as shown in Fig.6. The current slewing rate of phase A can be deduced as follow

$$\frac{di_{a3}}{dt} = \frac{2U_{dc}}{3l_a} + \frac{e_b + e_c - 2e_a}{3l_a} \quad (8)$$

During the PWM period T_s, the acting time of voltage vectors are defined as $(1-d)*T_s$, $(d-d_T)*T_s$ and $d_T^*T_s$ respectively, and corresponding current variation of phase A can be obtained as

$$\begin{cases} \Delta i_{a1} = (\dfrac{e_b + e_c - 2e_a}{3l_a})(1 - d)T_s \\ \Delta i_{a2} = (\dfrac{U_{dc}}{3l_a} + \dfrac{e_b + e_c - 2e_a}{3l_a})(d - d_T)T_s \\ \Delta i_{a3} = (\dfrac{2U_{dc}}{3l_a} + \dfrac{e_b + e_c - 2e_a}{3l_a})d_T T_s \end{cases} \quad (9)$$

The total current variation of non-commutating phase A in the PWM period can be expressed as follow.

$$\begin{aligned} \Delta i &= \Delta i_{a1} + \Delta i_{a2} + \Delta i_{a3} \\ &= (\frac{U_{dc}}{3l_a} + \frac{e_b + e_c - 2e_a}{3l_a})(d - d_T)T_s \\ &\quad + (\frac{e_b + e_c - 2e_a}{3l_a})(1 - d)T_s \\ &\quad + (\frac{2U_{dc}}{3l_a} + \frac{e_b + e_c - 2e_a}{3l_a})d_T T_s \end{aligned} \quad (10)$$

With the aim to maintain the current of the non-commutating phase A, the total current variation of phase A should be 0 in the PWM period. The DC-link voltage U_{dc} and all the parameters of the BLDCM could be assumed as unconverted values in the high-frequency PWM period, then, the duty cycle d_T could be calculated as

$$d_T = \frac{2e_a - e_b - e_c}{U_{dc}} - d = \frac{e_{ab} + e_{ac}}{U_{dc}} - d \quad (11)$$

where, e_{ab} and e_{ac} are the corresponding line back EMF respectively, and $e_{ab} + e_{ac}$ is the positive and maximum value in the commutation interval from A+B− to A+C−. As aforementioned, with restrictions of d_T, which should be

smaller than d, and all the duty cycle should be smaller than 1, the trajectory map of the duty cycle for the TVVI can be depicted as the gray triangle in the following Fig.7.
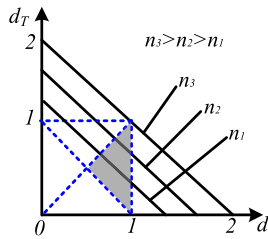

FIGURE 7. The trajectory map of duty cycle d_T versus d.

As the amplitude of $e_{ab} + e_{ac}$ is proportional to the speed, n_3 is the maximum speed for the TVVI method where $e_{ab} + e_{ac} = 2U_{dc}$. When the speed is lower to n_1, and $U_{dc} > e_{ab} + e_{ac}$, the current of non-commutating phase could be regulated by the duty cycle of the corresponding switches, and n_1 is the minimum speed where the TVVI method could be employed for the elimination for the commutation torque ripple. In other words, d_T should be set as 0 when the speed of BLDCM is lower than a certain value.

In the next commutation interval from A+C− to B+C−, where phase A is the outgoing phase, phase B is the incoming phase, and phase C is the non-commutating phase. The proposed TVVI method could be adopted for the current regulation of phase C, and the duty cycle for the injected three-phase voltage vector could be deduced as follow

$$d_T = \frac{e_a + e_b - 2e_c}{U_{dc}} - d = \frac{e_{ac} + e_{bc}}{U_{dc}} - d \quad (12)$$

where, $e_{ac} + e_{cc}$ is positive and maximum in the commutation interval from A+C− to B+C−. Furthermore, the duty cycle expression for the TVVI in other commutation intervals are similar to the above equations in the PWM-ON pattern, and the general duty cycle can be written as

$$d_T = \frac{|2e_x - e_y - e_z|}{U_{dc}} - d = \frac{e_{xy} + e_{xz}}{U_{dc}} - d \quad (13)$$

where, subscript x, y, and z refer to the corresponding non-commutating phase, outgoing phase and incoming phase, respectively. It can be seen that the duty cycle for TVVI method is determined by the sum of the line voltage of back EMF and the output of the inner DPC loop, and it could be calculated in each switching period and exploited for the mitigation of commutation torque ripple.

B. EXTENDED TVVI IN OTHER PWM PATTERNS

As explained above, the duty cycle calculation of three-phase voltage vector for the commutation torque reduction is on the basis of PWM-ON pattern. The three-phase voltage vector injection method could also be extended to the other PWM patterns, such as ON-PWM, H-PWM-L-ON, H-ON-L-PWM.

Since the chopping switches are different in the ON-PWM pattern, in the commutation interval from A+B− to A+C−,

S_1 is working in the chopping mode, and S_6 keeps turning on, the three-phase voltage vector A+B−C− in injected in the commutation interval. Then, the current slewing rate of non-commutating phase A by the different active voltage vectors can be expressed as

$$\begin{cases} \dfrac{di_{a1}}{dt} = -\dfrac{U_{dc}}{3l_a} + \dfrac{e_b + e_c - 2e_a}{3l_a} \\ \dfrac{di_{a2}}{dt} = \dfrac{U_{dc}}{3l_a} + \dfrac{e_b + e_c - 2e_a}{3l_a} \\ \dfrac{di_{a3}}{dt} = \dfrac{2U_{dc}}{3l_a} + \dfrac{e_b + e_c - 2e_a}{3l_a} \end{cases} \quad (14)$$

According to the aim of the total current variation, which should be equal to zero, the duty cycle of the injected three-phase voltage vector is calculated as.

$$d_T = 1 - 2d + \frac{2e_a - e_b - e_c}{U_{dc}} = 1 - 2d + \frac{e_{ab} + e_{ac}}{U_{dc}} \quad (15)$$

Likewise, the general duty cycle expression equation in ON-PWM pattern could be written as

$$d_T = 1 - 2d + \frac{e_{xy} + e_{xz}}{U_{dc}} \quad (16)$$

From the equation (13) and (16), it can be noted that when the non-commutating phase keeps on, the duty cycle of the TVVI is identical with the equation (13), whereas, when the non-commutating phase works in chopping mode, the duty cycle of the TVVI is in accordance with the equation (16). Therefore, the duty cycle for TVVI in the H-PWM-L-ON and H-ON-L-PWM patterns can be concluded in TABLE 1, where, the commutation intervals from A+B− to A+C−, A+C− to B+C−, B+C− to B+A−, B+A− to C+A−, C+A− to C+B−, and C+B− to A+B− are defined as CI_1, CI_2, CI_3, CI_4, CI_5 and CI_6 respectively, and duty cycle of the TVVI in each commutation interval are represented by (13) and (16) respectively.

TABLE 1. Duty cycle of TVVI in different PWM patterns.

| Duty cycle	CI_1	CI_2	CI_3	CI_4	CI_5	CI_6
PWM-ON	(13)	(13)	(13)	(13)	(13)	(13)
ON-PWM	(16)	(16)	(16)	(16)	(16)	(16)
H-PWM-L-ON	(13)	(16)	(13)	(16)	(13)	(16)
H-ON-L-PWM	(16)	(13)	(16)	(13)	(16)	(13)

IV. INCORPORATED CONTROL STRATEGY FOR BLDCM

In the conduction period of the rectangular phase currents control scheme for BLDCM, and, the output torque can be expressed as

$$T_e = \frac{(e_m - e_n)i_m}{\omega_e} = \frac{e_{mn}i_m}{\omega_e} \quad (17)$$

where, e_m, e_n are the back EMFs of the conducting phases, and e_{mn} indicates the line-voltage of the corresponding phases, i_m is the amplitude of the square-wave current, ω_e represents the electrical angular velocity. Since the non-idealized

BLDCM has the sinusoidal back EMF waveforms, the rectangular currents will cause cyclic torque ripple according to the line-voltage curve, and the output torque T_e is shown as the red dot line in Fig.8.
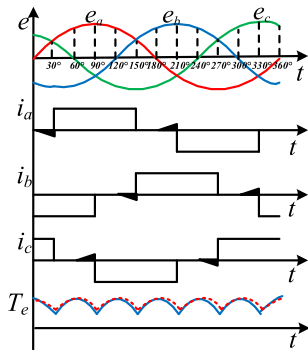
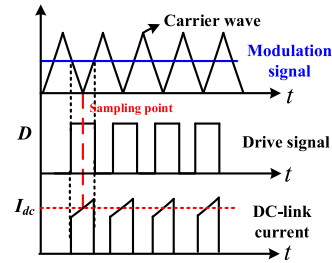**FIGURE 8.** Schematic diagram of the phase currents and output torque of BLDC with non-ideal back-EMF.

From the recent research literature for BLDCM, the PWM-ON pattern employing single switch chopping has been indicated as the optimal PWM method with the less switching loss and low current ripples for BLDCM. However, the unexpected conduction due to the voltage fluctuation of the neutral point leads to the current tails of each phase in the non-conducting phase illustrated in Fig.8. It deteriorates the torque ripples and mean value of torque in the conduction period, and the output torque is depicted as the blue full line. Although the PWM-ON-PWM pattern could be effective to eliminate the phenomenon of the current tail, the extra operating modes and section partition method increase the control complexity and switching loss. Therefore, the PWM-ON pattern is selected as the benchmark for the torque ripple analysis of BLDC in this paper.

From the equation(17), it can be seen that the instantaneous torque close-loop instead of current is an effective way to eliminate the conduction torque ripple, however the low pass filter for sampling the back EMF waveform and estimated value error of the rotor position for feedback torque calculation not only increase the control complex but also result in the deviation of the command torque.

A. DIRECT POWER CONTROL FOR CONDUCTION TORQUE RIPPLE

A simplified direct power control method is employed herein for the reduction of commutation torque ripple instead of the direct torque control. The proposed directed power measurement is implemented in the PWM switching period, where the rotor speed could be assumed as a constant value, and the input power of VSI is calculated by the detection of input voltage and average current in the switching period. The output power of BLDCM is proportional to the system efficiency η, which could also be assumed as constant due to the steady operation condition of constant speed and the load of BLDCM. Thus, the output power could be utilized as the feedback in the closed-loop control instead of current.

In the steady-state, the output torque of BLDCM could be maintained constant, then, the output torque could also be constant due to the negligible speed variation in the switching period.

FIGURE 9. Schematic diagram of the average current sampling method.

Fig.9 depicts the interrupted waveforms of input dc-link current of the VSI in the PWM-ON pattern in order to get the mean value of the input current, the sampling point should be selected at the lowest point of the triangle carrier wave, in other words, the AD conversion of dc-link current actives when the PWM timer underflows, then the means values of the current in the PWM duty cycle is obtained, and the average dc-link current in the PWM switching cycle is deduced as $I_{dc}^* d$, where d stands for the duty cycle of the PWM cycle, and I_{dc} is the mean value of the output current of battery.

The feedback average power could be calculated as

$$\overline{P} = \frac{U_{dc} \int i_{dc} dt}{t_s} = U_{dc} \cdot I_{dc} \cdot d \tag{18}$$

where, U_{dc} and i_{dc} are the voltage and output current of the battery for the driving system respectively. t_s indicates the switching period. Then, the DPC method could be adopted in double-loop control the BLDCM instead of the traditional current-loop, and only one dc bus current sensor is necessary for the cost reduction of the driving system. In the constant speed and constant load operation condition, the torque ripple in the conduction mode could be eliminated.

B. INCORPORATED TORQUE RIPPLE MITIGATION METHOD

Fig.10 shows the schematic diagram of the proposed incorporated torque ripples mitigation method of DPC and TVVI. The traditional speed control is utilized as the outer loop for the BLDCM driving system, and the DPC is employed to instead of the current control for the elimination of the conduction torque ripple due to the non-ideal back EMF of BLDCM.

The output duty cycle d of the inner loop is for the calculation of the feedback instantaneous input power and is also for the duty cycle d_T in terms of the equation (13) or (16). Although the back EMF sampling module should be added for the calculation of d_T, due to the sinusoidal waveforms of the back EMF of BLDCM, the amplitudes could be estimated by the speed directly, then, the TVVI methods in different PWM patterns could be implemented for the mitigation of the
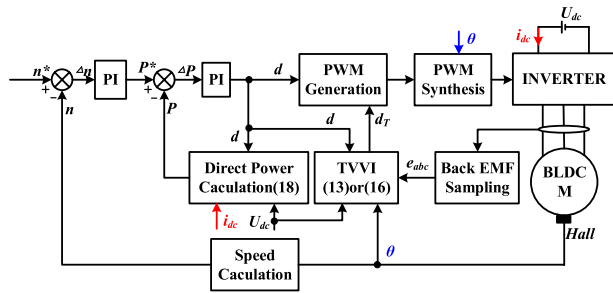
FIGURE 10. Schematic diagram of the incorporated control strategy.

commutation torque ripple without any extra hardware circuits. Thus, both conduction and commutation torque ripples of BLDCM could be mitigated by the proposed incorporated control strategy.

V. SIMULATION RESULTS

The simulation module of BLDCM with sinusoidal back EMF in the traditional current-loop control, DPC methods and proposed incorporated control strategy are computed for the comparison, and the parameters of the proposed BLDCM system are shown in TABLE 2.

TABLE 2. Parameters of the proposed BLDCM.

Parameters	Value
Rate speed/r/min	3000
Self-inductance of phase winding /mH	0.3
Resistance of phase winding/Ω	1.25
Pole pairs of the rotor	5
Switching frequency/kHz	15
Rotational inertia/ kg·m²	0.1
Dc-link voltage/V	160
Coefficient of back EMF/V/rpm	0.035
Load/Nm	1

A. COMPARISON RESULTS OF BLDCM WITH DIFFERENT METHODS

Fig.11 shows the simulation waveforms of currents and output torque of BLDCM with the traditional current-loop control strategy, the phase currents are chopped to follow the command rectangular current of 2.2A in PWM-ON pattern. In the conduction period, the conduction torque ripple reaches 0.5Nm, nearly 50% of the mean value of 1Nm. Comparison to the simulation waveforms in the DPC method in Fig.12, it can be noted that the phase currents are not idealized rectangular, and they vary to compensate the back EMF, then the output power remains constant, and the torque ripple in the conduction period could be limited in 0.05Nm or less, almost 90% improvement for the conduction torque ripple. However, the DPC method has less affection on the commutation torque ripple with the value of 0.4Nm. Fig. 13 shows the simulation waveforms of three-phase currents and output torque

with the proposed incorporated method of DPC and TVVI. The phase currents of BLDC are tracking the trajectory of the sine curve of back EMF due to the DPC method, and the currents of incoming and outgoing phase are all chopping for the constant current of non-commutating phase, although the commutation interval has been extended, the torque ripple in the commutation interval could be eliminated. Furthermore, the output torque ripple of BLDC under the proposed control method could be reduced to be 0.05Nm, which is only 12.5% of the original torque ripple, then the high torque performance of BLDCM could be achieved.

The simulation verifications of the proposed torque ripples mitigation method for the different PWM patterns of ON-PWM and H-PWM-L-ON are accomplished in this paper. The simulation parameters are also identical to TABLE 2. Fig.14 illustrates the comparison simulation results of three-phase currents and output torque of BLDCM with the current-loop and the proposed incorporate control method in the ON-PWM pattern. The waveforms in the left column are with the traditional current-loop control strategy, and those in the right column are with the proposed incorporated torque ripples mitigation method. As the non-commutating phase works in the chopping mode, and it is different from that in the PWM-ON patterns, the duty cycle for TVVI is in terms of equation(16). In the conduction interval, the steady torque is about 0.5Nm under the conventional control method, and the commutation torque ripple is also 0.5Nm, which is larger than that in the PWM-ON pattern. After the implementation of the torque ripple mitigation method, the conduction torque ripple could be reduced as 0.05Nm or less, which is only 10% of the original value, and the commutation torque ripple is only 0.1Nm.

Fig.15 depicts the comparison results of the phase currents, output torque and driving signals in the H-PWM-L-ON pattern with and without the proposed torque ripple mitigation method. It can be seen that the original conduction torque ripple of 0.5Nm and commutation torque ripple of 0.4Nm in the current-loop control strategy could be reduced to 0.1Nm or less by the implementation of the proposed torque ripple mitigation method. The duty cycle d_T for the different commutation intervals in H-PWM-L-ON pattern could be obtained for the TABLE 1. Furthermore, the simulation results of the BLDCM in the H-ON-L-PWM are identical with that in H-PWM-L-ON pattern, and the duty cycle d_T for TVVI is shown in TABLE 1, thus they are not listed in the paper for the lack of space.

B. WIDE SPEED RANGE PERFORMANCE

Simulation results of the proposed control strategy for the BLDCM drive system with respect to the different command speed of 2500r/min, 1500r/min and 500r/min are illustrated in Fig.16, the commutation and conduction torque ripples could be mitigated effectively. In the operation speed of 2500r/min and 1500r/min, the current of the outgoing phase is working in chopping mode due to the three-phase voltage vector injection. While, when BLDC operated at the low

(a) Three-phase currents

(b) Output torque

FIGURE 11. Simulation waveforms of BLDCM with the current-loop control method in PWM-ON pattern.

(a) Three-phase currents

(b) Output torque
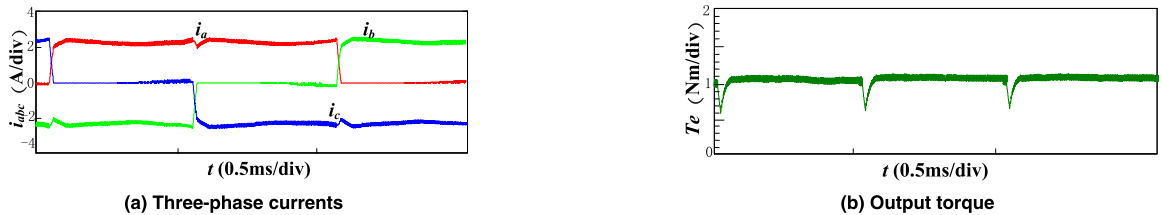
FIGURE 12. Simulation waveforms of BLDCM with the DPC method in PWM-ON pattern.
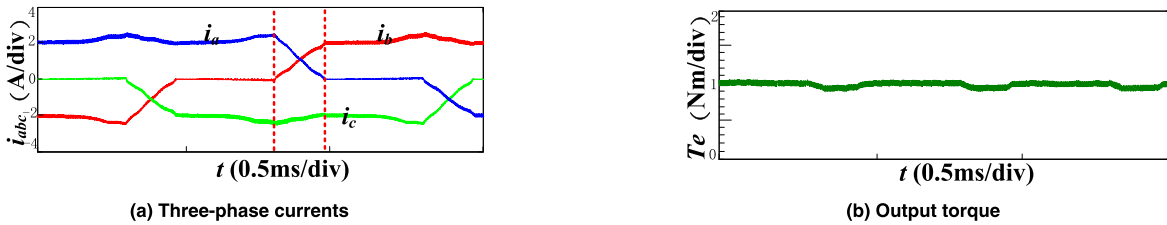

(a) Three-phase currents

(b) Output torque

FIGURE 13. Simulation waveforms of BLDCM with the incorporated control method in PWM-ON pattern.

(a) With current-loop control method

(b) With incorporated method
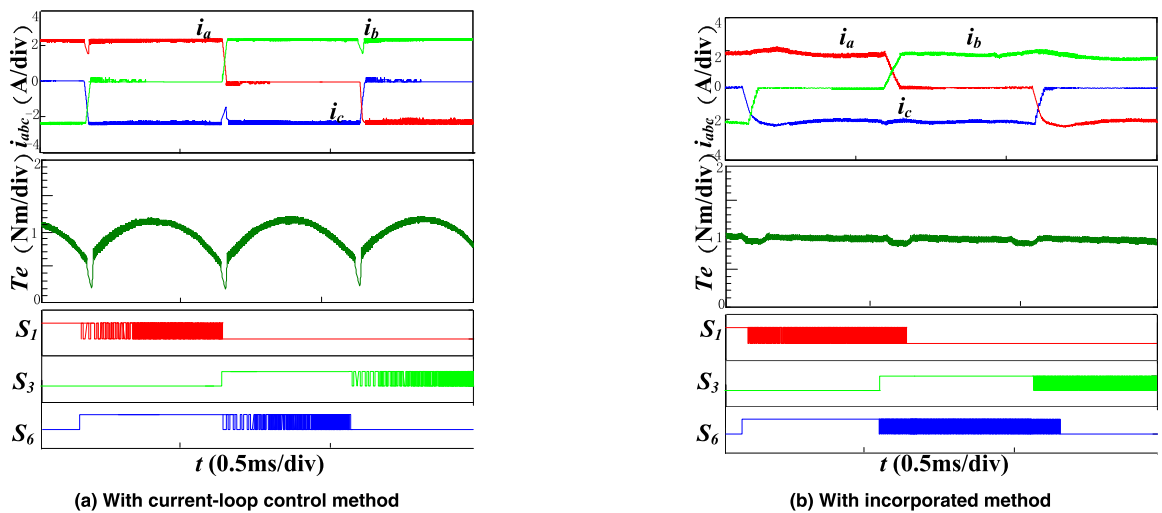
FIGURE 14. Simulation waveforms comparison of phase current, output torque and driving signals in ON-PWM pattern with and without the incorporated control method.

speed, and $(|e_{xy} + e_{xz}|/U_{dc}\text{-}d) < 0$, d_T is limited to be 0 due to the Fig.6. The current of outgoing phase declines directly to be zero without any chopping modulation as the calculated duty cycle of the injected three-phase voltage vector is 0, the torque ripple could be mitigated by the DPC control strategy directly. From the simulation results, the conduction torque ripple could be restricted to be less than 0.1Nm, and the commutation torque ripple is limited in 0.05Nm, and the proposed torque ripple mitigation method could be extended to the whole speed range of BLDC without any modulation switching method from low speed to high speed, the higher output performance of BLDCM drives is achieved.

(a) With current-loop control method   (b)With incorporated method
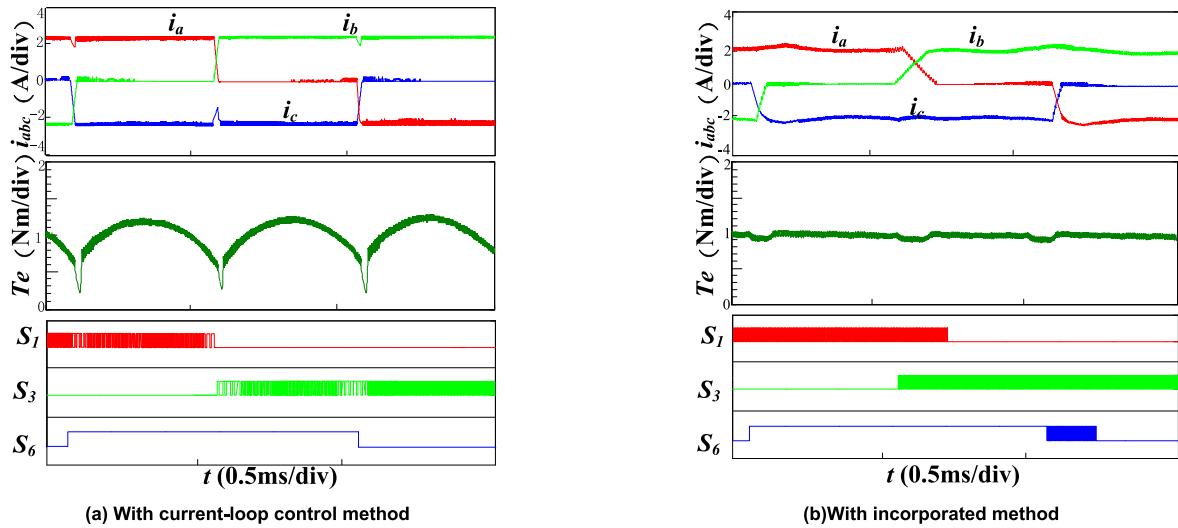
FIGURE 15. Simulation waveforms comparison of phase current, output torque and driving signals in H-PWM-L-ON pattern with and without the incorporated control method.

(a)n=2500r/min

(b)n=1500/min

(c)n=500r/min
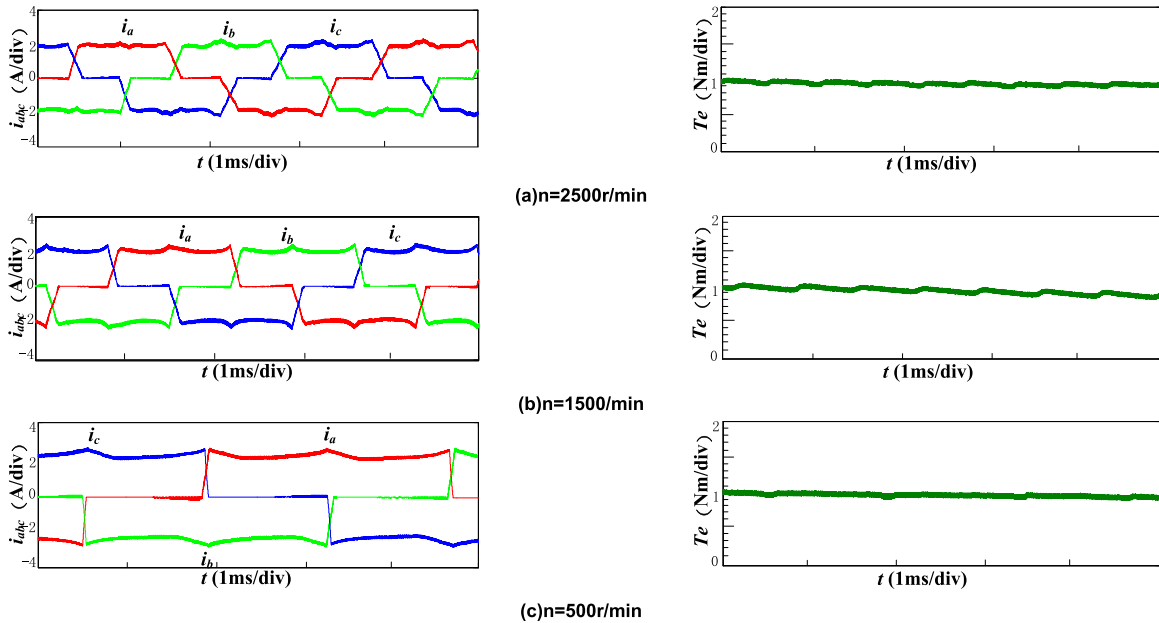
FIGURE 16. Simulation waveforms of phase current and output torque of BLDCM at different speeds in PWM-ON pattern.

VI. EXPERIMENT RESULTS

The prototype of the BLDCM driving system shown in Fig.17 is built for the validation of the proposed control strategy. The controller is based on the DSP of TMS320LF2812 and CPLD of ISP1032, and the parameters of the tested BLDCM is as same as TABLE 2. Fig.18 shows the sinusoidal waveforms of line back EMF waveforms of the BLDCM.

A. EXPERIMENT RESULTS COMPARISON OF BLDCM WITH DIFFERENT METHODS

For the compassion, he traditional current-loop control method, DPC method, and the proposed incorporated control

strategy are all accomplished in the same condition to verify the performance of the torque ripples mitigation, where the output torque is calculated based on the back EMF estimation and phase currents detection. Fig.19 shows the experiment waveforms of BLDCM with the traditional current-loop control method in PWM-ON pattern, the command phase current is 2.2A and the load is 1Nm at the speed of 3000r/min, it is obvious that the commutation and conduction torque ripples are both almost 0.4Nm, where the output torque is calculated by the DSP based on the back EMF and phase currents of BDLCM, and it is output to the oscilloscope by the DA converter.
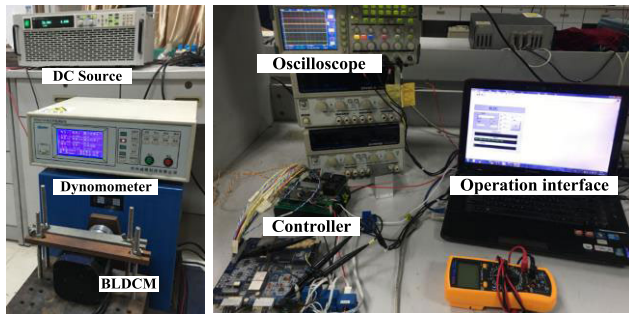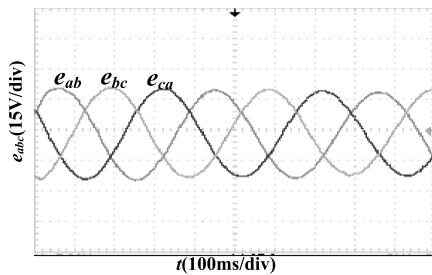
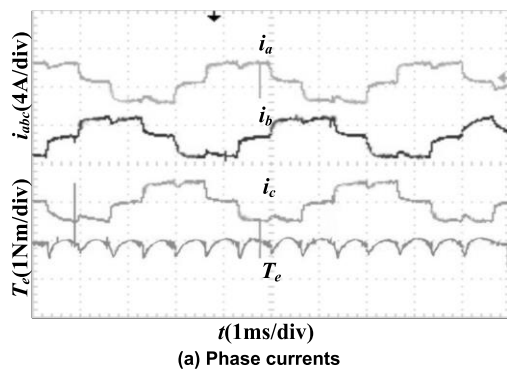**FIGURE 18.** Experiment waveforms of back EMF of the tested BLDCM.

With the only DPC control method for BLDCM, it can be seen that the conduction torque ripple could be eliminated effectively, while, the commutation torque ripple is

still 0.4Nm shown in Fig.20. Fig.21 depicts the current and output torque waveforms of BLDCM with the proposed incorporated control strategy, it can be observed that all the torque ripples could be eliminated to be less than 0.1Nm, and the phase currents follow the sinusoidal waveforms in each conduction period to mitigated the conduction torque ripple, and in the commutation interval, commutation torque ripple could be mitigated by the TVVI method effectively.

In order to verify the universal applicability of the proposed incorporated torque ripples mitigation method for BLDCM in different PWM patterns. The experiment waveforms comparison for the output torque performance in the typical ON-PWM and H-PW-L-ON patterns are given in Fig. 22 and 23. In accordance with the inner DPC control and duty cycle calculation for TVVI in TABLE 1, the output torque ripple of the BLDCM in these two different PWM patterns could be limited to be lower than 0.1Nm. It can be concluded from these experiment results that the BDLCM with the proposed torque ripples mitigation method could have high output torque performance and could be extended to the other applications where the torque ripples are the critical factors.

B. EXPERIMENT RESULTS IN DIFFERENT SPEEDS
The experiment results of the BLDCM at different speed are illustrated in Fig.24. The proposed incorporated torque ripples mitigation method is effective in the whole speed
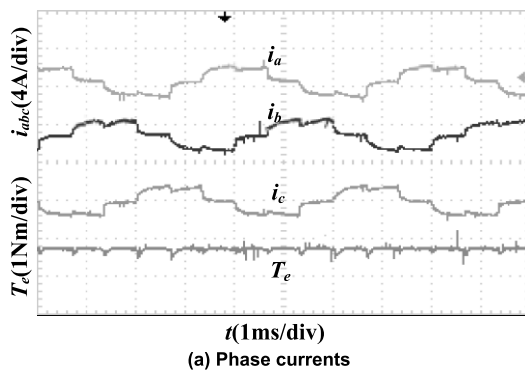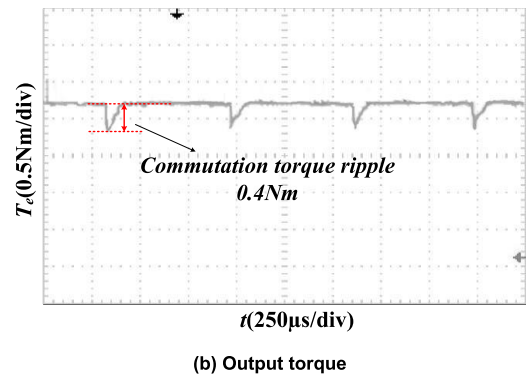

(a) Phase currents
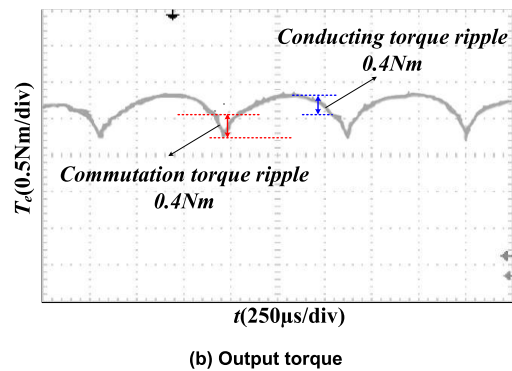
(b) Output torque

FIGURE 19. Experiment waveforms of BLDCM with the current-loop control method in PWM-ON pattern.

(a) Phase currents

(b) Output torque

FIGURE 20. Experiment waveforms of BLDCM with the DPC control method in PWM-ON pattern.
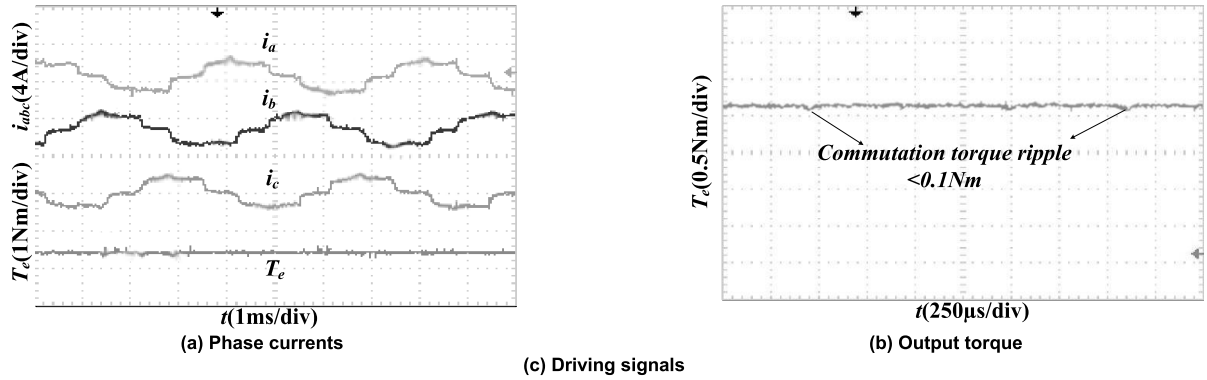
(a) Phase currents

(c) Driving signals

(b) Output torque

FIGURE 21. Experiment waveforms of BLDCM with incorporated control strategy in PWM-ON pattern.

(a) Tradition current-loop control method

(b)proposed incorporated control strategy
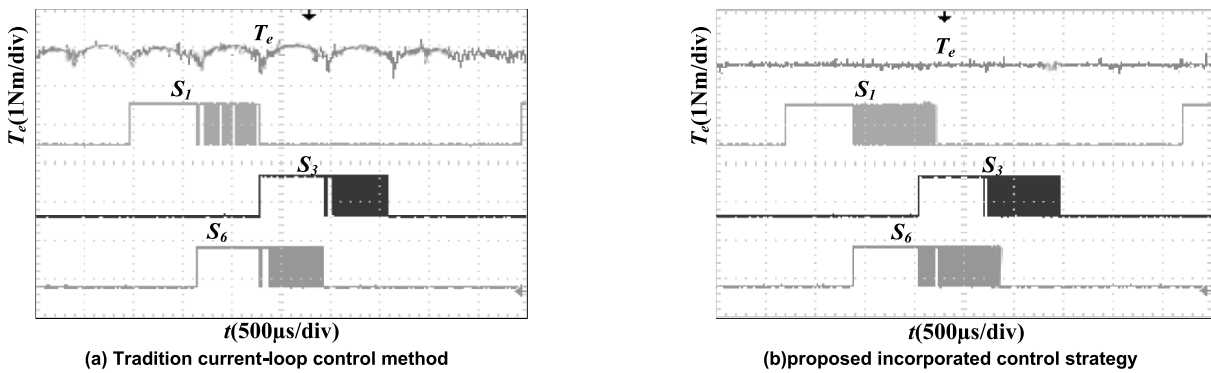
FIGURE 22. Experiment waveforms comparison of output torque and driving signals in ON-PWM pattern.

(a) Tradition current-loop control method

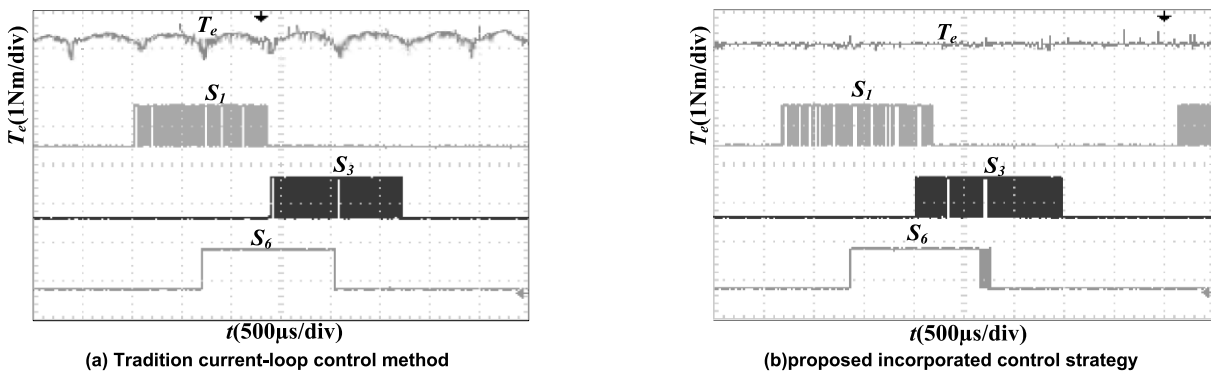(b)proposed incorporated control strategy

FIGURE 23. Experiment waveforms comparison of output torque and driving signals in H-PWM-L-ON pattern.

range from 500r/min to 2500r/min, the effect of TVVI could be found in the driving signal waveforms. The duty cycle for TVVI is calculated as 0 when the speed is 500r/min, and there is no TVVI for BLDCM, however, the output torque ripple could still be eliminated by the proposed incorporated control strategy. The experiments results of BLDCM at different speeds are in accordance with the simulation results in Fig.16.

The experiment results of the dynamic performance of the proposed BLDCM drives with the incorporated torque ripples mitigation method are shown in Fig.25. Fig.25(a) shows the waveforms of speed, output torque and phase currents

when the reference speed step up from 500rpm to 3000rpm, where the response time of the driving system is about 75ms, and in the dynamic procedure there is a tiny output torque variation of 0.1Nm and the phase currents could track the reference values quickly. Fig.25(b) depicts the load changing results of BLDCM from 0.5Nm to 1Nm at the constant speed of 3000rpm, where the response time is limited in 5ms, and there is only a small speed drop less than 25rpm in the dynamic procedure. These experiment results verify that the proposed BLDCM drive with the proposed torque ripples mitigation method has an excellent dynamic performance.
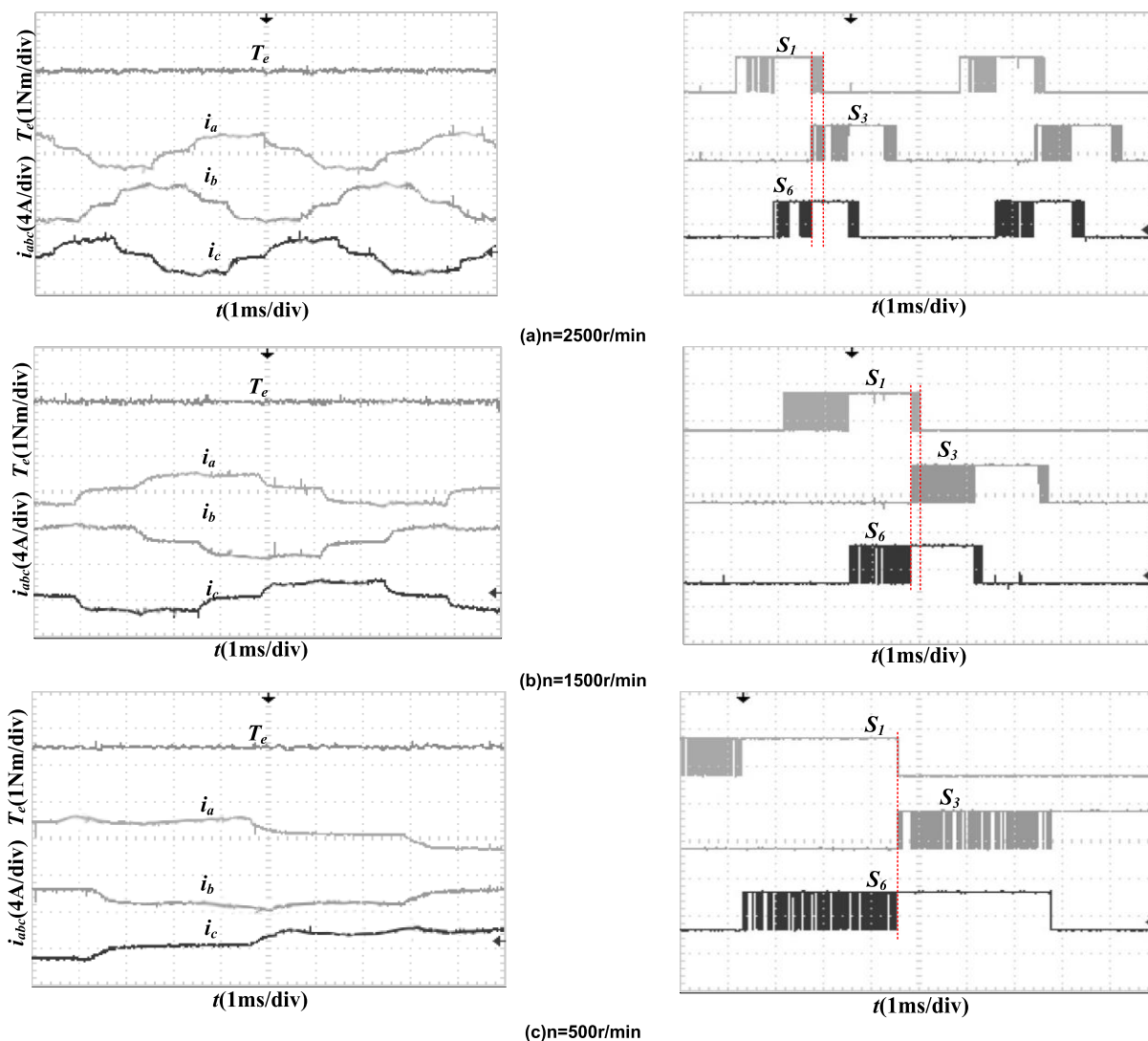
(a)n=2500r/min

(b)n=1500r/min

(c)n=500r/min

FIGURE 24. Experiment waveforms of phase current and output torque of BLDCM at different speeds in PWM-ON pattern.

(a) Speed step up from 500rpm to 3000rpm

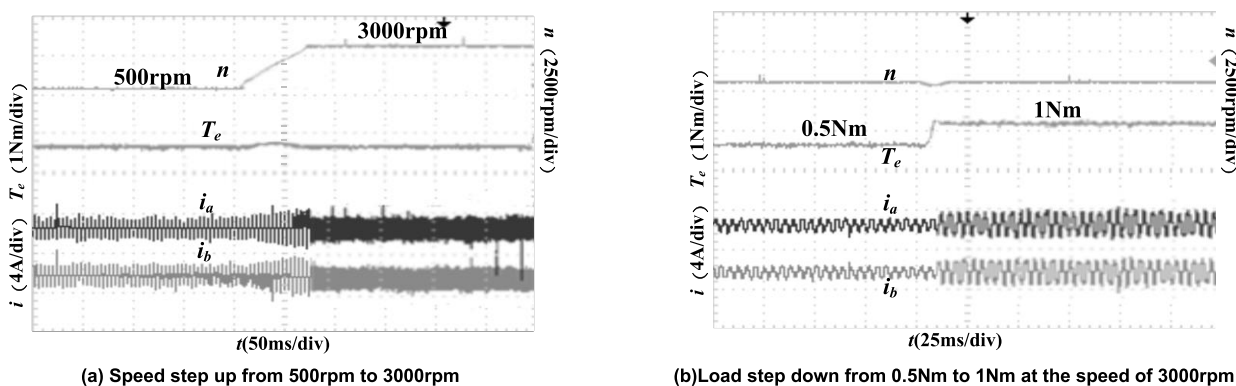(b)Load step down from 0.5Nm to 1Nm at the speed of 3000rpm

FIGURE 25. Experiment waveforms of the BLDCDM under the speed and load changing conditions.

VII. CONCLUSION

In this manuscript, an incorporated control strategy of commutation and conduction torque ripples mitigation for BLDCM with the sinusoidal back EMF in household appliances is proposed. Unlike the conventional separated analysis of the commutation and conduction torque ripples,

a combined torque ripples analysis depending on the stator flux linkage trajectory is introduced. A three-phase voltage vector injection(TVVI) method is designed and implemented in the commutation interval to compensate the sharp dips of the stator flux trajectory for the mitigation of the commutation torque ripple, then, a simple DPC is employed as inner-loop with the specific dc-link current sampling method to replace the traditional current-loop, and the desired waveforms of currents could be obtained for the conduction torque ripple mitigation. Moreover, the TVVI and DPC control schemes are combined together to achieve the torque ripples of less than 0.1Nm, which is only 12.5% of that in the traditional current-loop control method. From the results of the comparison tests, the proposed method ensures a significant reduction of the commutation and conduction torque ripple for BLDCM with the low-cost property, and the effectiveness and feasibility have been extended to the other PWM patterns and wide speed range. Thus, BLDCM with the improved higher torque performance can also be applied to the other applications, where, the cost and torque ripples are of great concern.

REFERENCES

[1] R. Carlson, M. Lajoie-Mazenc, and J. C. D. S. Fagundes, "Analysis of torque ripple due to phase commutation in brushless DC machines," *IEEE Trans. Ind. Appl.*, vol. 28, no. 3, pp. 632–638, May 1992.

[2] Y.-K. Lin and Y.-S. Lai, "Pulsewidth modulation technique for BLDCM drives to reduce commutation torque ripple without calculation of commutation time," *IEEE Trans. Ind. Appl.*, vol. 47, no. 4, pp. 1786–1793, Jul./Aug. 2011.

[3] J. Shi and T.-C. Li, "New method to eliminate commutation torque ripple of brushless DC motor with minimum commutation time," *IEEE Trans. Ind. Electron.*, vol. 60, no. 6, pp. 2139–2146, Jun. 2013.

[4] F. Yang, C. Jiang, A. Taylor, H. Bai, A. Kotrba, A. Yetkin, and A. Gundogan, "Design of a high-efficiency minimum-torque-ripple 12-V/1-kW three-phase BLDC motor drive system for diesel engine emission reductions," *IEEE Trans. Veh. Technol.*, vol. 63, no. 7, pp. 3107–3115, Sep. 2014.

[5] C. K. Lad and R. Chudaman, "Simple overlap angle control strategy for commutation torque ripple minimisation in BLDC motor drive," *IET Electr. Power Appl.*, vol. 12, no. 6, pp. 797–807, Jul. 2018.

[6] S. S. Bharatkar, R. Yanamshetti, D. Chatterjee, and A. K. Ganguli, "Dual-mode switching technique for reduction of commutation torque ripple of brushless dc motor," *IET Electr. Power Appl.*, vol. 5, no. 1, pp. 193–202, Jan. 2011.

[7] Y. Cao, T. Shi, X. Niu, X. Li, and C. Xia, "A smooth torque control strategy for brushless DC motor in braking operation," *IEEE Trans. Energy Convers.*, vol. 33, no. 3, pp. 1443–1452, Sep. 2018.

[8] W. Chen, Y. Liu, X. Li, T. Shi, and C. Xia, "A novel method of reducing commutation torque ripple for brushless DC motor based on Cuk converter," *IEEE Trans. Power Electron.*, vol. 32, no. 27, pp. 5497–5508, Jul. 2017.

[9] V. Viswanathan and S. Jeevananthan, "Hybrid converter topology for reducing torque ripple of BLDC motor," *IET Power Electron.*, vol. 10, no. 12, pp. 1572–1587, Oct. 2017.

[10] X. Li, C. Xia, Y. Cao, W. Chen, and T. Shi, "Commutation torque ripple reduction strategy of Z-source inverter fed brushless DC motor," *IEEE Trans. Power Electron.*, vol. 31, no. 11, pp. 7677–7690, Nov. 2016.

[11] V. Viswanathan and J. Seenithangom, "Commutation torque ripple reduction in the BLDC motor using modified SEPIC and three-level NPC inverter," *IEEE Trans. Power Electron.*, vol. 33, no. 1, pp. 535–546, Jan. 2018.

[12] H. Lu, L. Zhang, and W. Qu, "A new torque control method for torque ripple minimization of BLDC motors with un-ideal back EMF," *IEEE Trans. Power Electron.*, vol. 23, no. 2, pp. 950–958, Mar. 2008.

[13] Z. Q. Zhu and J. H. Leong, "Analysis and mitigation of torsional vibration of PM brushless AC/DC drives with direct torque controller," *IEEE Trans. Ind. Appl.*, vol. 8, no. 4, pp. 1296–1306, Jul/Aug. 2012.

[14] M. Masmoudi, B. El Badsi, and A. Masmoudi, "DTC of B4-inverter-fed BLDC motor drives with reduced torque ripple during sector-to-sector commutations," *IEEE Trans. Power Electron.*, vol. 29, no. 9, pp. 4855–4865, Sep. 2014.

[15] K. D. Carey, N. Zimmerman, and C. Ababei, "Hybrid field oriented and direct torque control for sensorless BLDC motors used in aerial drones," *IET Power Electron.*, vol. 12, no. 3, pp. 438–449, Mar. 2019.

[16] S. M. Shakouhi, M. Mohamadian, and E. Afjei, "Torque ripple minimisation control method for a four-phase brushless DC motor with non-ideal back-electromotive force," *IET Electr. Power Appl.*, vol. 7, no. 5, pp. 360–368, May 2013.

[17] C. Xia, Y. Wang, and T. Shi, "Implementation of finite-state model predictive control for commutation torque ripple minimization of permanent-magnet brushless DC motor," *IEEE Trans. Ind. Electron.*, vol. 60, no. 3, pp. 896–905, Mar. 2013.

[18] Y. Zhang and C. Qu, "Direct power control of a pulse width modulation rectifier using space vector modulation under unbalanced grid voltages," *IEEE Trans. Power Electron.*, vol. 30, no. 10, pp. 5892–5901, Oct. 2015.

[19] A. H. Niasar and M. Moazzemi, "Design and implementation of direct power control system for brushless DC generator in standalone DC applications," *Electr. Power Compon. Syst.*, vol. 45, no. 7, pp. 752–762, May 2017.

[20] A. G. de Castro, W. C. A. Pereira, T. E. P. Almeida, C. M. R. de Oliveira, J. R. B. A. Monteiro, and A. A. de Oliveira, "Improved finite control-set model-based direct power control of BLDC motor with reduced torque ripple," *IEEE Trans. Ind. Appl.*, vol. 54, no. 5, pp. 4476–4484, Sep./Oct. 2018.

[21] H. Moghbeli, A. H. Niasar, and M. B. Shahrbabak, "Direct power control of brushless DC motor drive," in *Proc. IEEE 23rd Int. Symp. Ind. Electron. (ISIE)*, Istanbul, Turkey, Jun. 2014, pp. 789–794.

[22] S.-Y. Jung, Y.-J. Kim, J. Jae, and J. Kim, "Commutation control for the low-commutation torque ripple in the position sensorless drive of the low-voltage brushless DC motor," *IEEE Trans. Power Electron.*, vol. 29, no. 11, pp. 5983–5994, Nov. 2014.

[23] T. Sheng, X. Wang, J. Zhang, and Z. Deng, "Torque-ripple mitigation for brushless DC machine drive system using one-cycle average torque control," *IEEE Trans. Ind. Electron.*, vol. 62, no. 4, pp. 2114–2122, Apr. 2015.

[24] C. Xia, Y. Xiao, W. Chen, and T. Shi, "Torque ripple reduction in brushless DC drives based on reference current optimization using integral variable structure control," *IEEE Trans. Ind. Electron.*, vol. 61, no. 2, pp. 738–752, Feb. 2014.

[25] J. K. Pandit, M. V. Aware, R. V. Nemade, and E. Levi, "Direct torque control scheme for a six-phase induction motor with reduced torque ripple," *IEEE Trans. Power Electron.*, vol. 32, no. 9, pp. 7118–7129, Sep. 2017.

[26] W. Jiang, H. Huang, J. Wang, Y. Gao, and L. Wang, "Commutation analysis of brushless DC motor and reducing commutation torque ripple in the two-phase stationary frame," *IEEE Trans. Power Electron.*, vol. 32, no. 6, pp. 4675–4682, Jun. 2017.

[27] J.-L. Ha, "Voltage injection method for three-phase current reconstruction in PWM inverters using a single sensor," *IEEE Trans. Power Electron.*, vol. 24, no. 3, pp. 767–775, Mar. 2009.
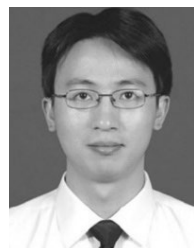
JIADAN WEI (M'10) was born in Danyang, China, in 1981. He received the B.S. and Ph.D. degrees in electrical engineering from the Nanjing University of Aeronautics and Astronautics (NUAA), Nanjing, China, in 2003 and 2009, respectively. From July 2016 to July 2017, he was a Visiting Scholar with the Power Electronics, Machine and Control Group (PEMC), University of Nottingham, U.K. Since 2009, he has been a member of the faculty with the Department of Electrical Engineering, NUAA, where he is currently an Associate Professor with the College of Automation Engineering.

His research interests include aircraft power systems, sensorless control of electric machine, and integrated motor and battery charger for electric vehicle.

PENG LIU was born in Nantong, China, in 1994. He received the B.S. degree in electrical engineering from the Nanjing University of Aeronautics and Astronautics, Nanjing, China, in 2017, where he is currently pursuing the M.S. degree in power electronics and drives.

His research interests include permanent magnet synchronous machine, and integrated motor and battery charger.

WENJIE TAO was born in Suqian, China, in 1996. He received the B.S. degree in electrical engineering from the Nanjing University of Aeronautics and Astronautics, Nanjing, China, in 2018, where he is currently pursuing the M.S. degree in power electronics and drives.

His research interests include open-winding permanent magnet synchronous machine and direct torque control.

• • •